ACS OMEGA

Article

Cite This: ACS Omega 2019, 4, 4176−4184

http://pubs.acs.org/journal/acsodf

Development of Acoustically Active Nanocones Using the Host−Guest Interaction as a New Histotripsy Agent

Tanzeel Ur Rehman,[†] Jennifer Khirallah,[‡] Erhan Demirel,[†] Justin Howell,[‡] Eli Vlaisavljevich,*[,‡] and Yasemin Yuksel Durmaz*[,†,§]

[†]Department of Biomedical Engineering, School of Engineering and Natural Sciences, and [§]Regenerative and Restorative Medicine Research Center (REMER), Istanbul Medipol University, Istanbul 34810, Turkey

[‡]Department of Biomedical Engineering and Mechanics, Virginia Polytechnic Institute and State University, Blacksburg 24061, United States

Supporting Information

ABSTRACT: Histotripsy is a noninvasive and nonthermal ultrasound ablation technique, which mechanically ablates the tissues using very short, focused, high-pressured ultrasound pulses to generate dense cavitating bubble cloud. Histotripsy requires large negative pressures (≥28 MPa) to generate cavitation in the target tissue, guided by real-time ultrasound imaging guidance. The high cavitation threshold and reliance on real-time image guidance are potential limitations of histotripsy, particularly for the treatment of multifocal or metastatic cancers. To address these potential limitations, we have recently developed nanoparticle-mediated histotripsy (NMH) where perfluorocarbon (PFC)-filled nanodroplets (NDs) with the size of ∼200 nm were used as cavitation nuclei for histotripsy, as they are able to significantly lower the cavitation threshold. However, although NDs were shown to be an effective histotripsy agent, they pose several issues. Their generation requires multistep synthesis, they lack long-term stability, and determination of PFC concentration in the treatment dose is not possible. In this study, PFC-filled nanocones (NCs) were developed as a new generation of histotripsy agents to address the mentioned limitations of NDs. The developed NCs represent an inclusion complex of methylated β-cyclodextrin as a water-soluble analog of β-cyclodextrin and perfluorohexane (PFH) as more effective PFC derivatives for histotripsy. Results showed that NCs are easy to produce, biocompatible, have a size <50 nm, and have a quantitative complexation that allows us to directly calculate the PFH amount in the used NC dose. Results further demonstrated that NCs embedded into tissue-mimicking phantoms generated histotripsy cavitation "bubble clouds" at a significantly lower transducer amplitude compared to control phantoms, demonstrating the ability of NCs to function as effective histotripsy agents for NMH.

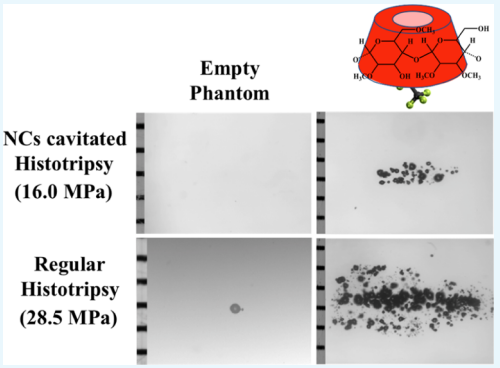

INTRODUCTION

Histotripsy is a noninvasive ultrasound (US) ablation technique, which mechanically ablates soft tissue (i.e., tumors) through acoustic cavitation mechanism. As a noninvasive and nonthermal technique, histotripsy uses very short, focused, high-pressured US pulses to fractionate the tissue.[1−4] When these US pulses interact with the water inside of the tissue, bubble clusters are nucleated, forming highly energetic microbubbles that expand to a size of >50 μm, and rapidly collapse, releasing energy into neighboring cells to mechanically fragment them to subcellular debris.[5,6] To generate this rapid bubble expansion and collapse in histotripsy, a high negative pressure threshold (≥28 MPa) is required to initiate cavitation.[7,8] Although histotripsy has shown its potential for many clinical applications including tumor ablation,[9−12] the efficacy of this technique is limited to situations in which a single target tumor can be identified and imaged before the treatment,[13] which is not possible for treating micrometastases or multiple tumor nodules. In addition, even with the image-guided system, the operator (clinician) needs to be extremely careful to accurately deliver US pulses to the focused area in order to avoid cavitation in healthy neighboring cells.

To deal with these limitations of targetability, selectivity, and high cavitation pressure, our group has recently developed nanoparticle-mediated histotripsy (NMH) as a novel ablation method to achieve selective tumor ablation. We developed NMH in order to significantly reduce the pressure required to selectively deliver histotripsy into the target tissue, enhance treatment efficiency, and allow the selective ablation of tumor cells while creating no effect on the neighboring healthy cells. NMH feasibility was demonstrated for the first time using perfluorocarbon (PFC)-filled nanodroplets (NDs) as a cavitation nuclei capable of reducing the histotripsy cavitation threshold.[14,15] These NDs were synthesized using a tri-block

Received: October 24, 2018
Accepted: February 14, 2019
Published: February 25, 2019

DOI: 10.1021/acsomega.8b02922
ACS Omega 2019, 4, 4176−4184

amphiphilic copolymer which encapsulates low-boiling point PFCs, either perfluoropentane (PFP) or perfluorohexane (PFH), as a result of their self-assembly into nanosized (~200 nm) droplets.[15] Phase transition of PFC in the core of NDs from liquid to gas through acoustic droplet vaporization forms nanobubbles under the US pulses, and these nanobubbles act like cavitation sites, and initiate the cavitation at lower cavitation threshold pressure.[13] Detailed studies about NMH showed[1,8,13,14,16,17] that using the NDs as the cavitation nuclei significantly lowered the cavitation threshold pressure (~7 MPa vs 28 MPa without droplets) and allowed cavitation to occur selectively only in the regions where the NDs localize at the lowered cavitation pressure value.[14] However, although NDs successfully addressed the selectivity and high cavitation threshold limitations of histotripsy, these first-generation histotripsy agents were associated with a few shortcomings that called for the development of new histotripsy agents. First of all, the synthesis of the NDs is complex, needs multiple steps, and requires expertise in the field of polymer chemistry. Second, the size of the NDs (~200 nm) is adequate for accumulation into the tumor tissue through an enhanced permeability and retention (EPR) effect, as supported by previous examples in the literature.[18−23] However, recent research has shown that a smaller size is better for EPR tumor accumulation, especially in early stage tumor formation.[24,25] Third, determining PFC concentration is important for NDs to be effective and consistent between the treatments. For prior NMH experiments, NDs concentration was determined using secondary concentration detection methods such as the nanoparticle tracking analysis system. This method provides concentration as a number of NDs/mL; however, the specific PFC amount in the NDs not only depends on solution concentration but also depends on size and size distribution of NDs. This means that every ND sample had a different amount of PFC, which makes it impossible to determine the exact concentration of PFC in the used solution. Lastly, stability of NDs was limited and requires cold storage conditions. Based on these limitations, there is a significant need for a new, practical, stable, and biocompatible histotripsy agent, which allows molecular-level isolation of PFC into nanosized (<50 nm) structures and provides concentration information of PFC without using secondary detection techniques.

Cyclodextrins (CDs) are Food and Drug Administration (FDA)-approved, biocompatible, nanosized molecules composed of glucopyranose units.[26,27] They are also known as cyclic oligosaccharides consisting of different numbers of cyclic sugar units. CDs used in the field of biomedicine are α-cyclodextrins, β-cyclodextrins (BCD), and γ-cyclodextrins consisting of six, seven, and eight glucopyranose units, respectively.[28] CDs have a conical shape with a hydrophilic exterior surface and a hydrophobic internal cavity.[29] They are known for their efficient role as a host molecule in an inclusion complex, and they have been reported to improve the solubility, bioactivity, and stability of many hydrophobic molecules.[30,31] Research has shown that among the above-mentioned CDs, BCD has been proven to be the most effective in forming inclusion complexes with PFCs because of the size compatibility of the PFC chain and the BCD cavity.[32] An early example shown by Hogen-Esch et al. presents characterization of an inclusion complex formed between BCD and a PFC alkyl chain containing water-soluble polymers.[33] Later, more work was published, for environmental purposes, to show the pollutant removal potential of the inclusion complex because some perfluorinated compounds, especially perfluoroalkyl carboxylic acid and perfluoroalkylsulfonates, are considered as a new class of persistent organic pollutants. In this regard, inclusion complex formation between BCD and different perfluoroalkyl carboxylic acids and their physicochemical characterization have been deeply studied.[34−36] The only example that used the BCD/PFC inclusion complex for an US-related application was recently published.[37] In this work, PFC used for US imaging (FC-77) was complexed with BCD at different PFC/BCD ratios. Even though US imaging potential of the complex was shown, the size of the complex was reaching the micron level depending on the PFC/BCD ratio, resulting in one PFC chain having two BCD molecules in a complex. To the best of our knowledge, there are no prior studies that use CD−PFC inclusion complexes for the histotripsy application.

The intramolecular hydrogen bonding of the secondary hydroxyl group of BCD leads to low aqueous solubility, which can be improved by increasing the temperature. However, this can cause problems such as evaporation of PFC from the system when BCD and volatile PFC derivatives attempt to form the inclusion complex. To increase water solubility of BCD at room temperature, it is necessary to substitute the hydrogens of hydroxyl groups by methoxy functions.[38] Among the other methods to increase water solubility of BCD, the methylation of BCD stands out as an economical and efficient method in the literature.[38] Moreover, methylated β-cyclodextrin (MCD) is used as an approved pharmaceutical component of certain drug delivery products.[39,40] Therefore, it appeared to be a good choice for our study because after methylation, the solubility increases and provides a more suitable environment for PFC complexation with higher efficiency. At the same time, it is still biocompatible, practical, and small as host molecules.

We hypothesized that hydrophobic PFH, as the most effective PFC for histotripsy,[13] can go into the hydrophobic cavity of the biocompatible, cone-shaped BCD derivatives in an aqueous environment to form an inclusion complex through host−guest interaction, resulting in solid "nanocones" (NCs) as a new generation histotripsy agent. Preparation of NCs is as easy as mixing two commercial and widely available compounds in an aqueous environment with a certain ratio and then collecting precipitated NCs through simple filtration. These NCs are expected to be of smaller size (<50 nm), and through complexed PFH, they can lower the cavitation threshold pressure for histotripsy. Moreover, the PFH amount in these NCs can be easily calculated, as it is directly proportional to the concentration of the NCs.

In this study, NCs, as the new histotripsy agent, were synthesized through host−guest interaction of FDA-approved, water-soluble derivatives of BCD (methylated BCD) and PFH through a practical and economical method with the size of less than 50 nm. The efficiency of inclusion complex formation was investigated, and quantitative complexation was achieved using better water-soluble derivative of BCD as a biocompatible and stable product. The amount of PFC in the obtained NCs was calculated, which acts as an important feature as it can be tuned differently for different treatments. Once all the physicochemical characterizations were performed, histotripsy parameters of NCs were studied to determine if NCs could effectively lower the cavitation threshold and act as an efficient histotripsy agent.

DOI: 10.1021/acsomega.8b02922
ACS Omega 2019, 4, 4176−4184

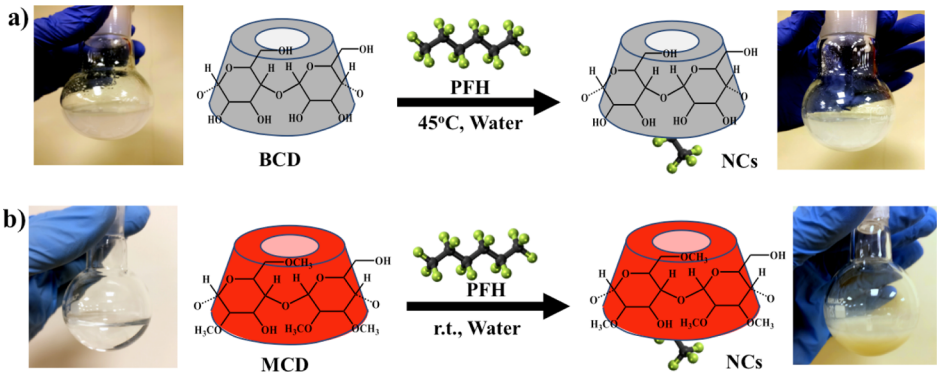

Figure 1. Schematic representation of synthesis of NCs through host−guest interaction between PFH and (a) BCD and (b) MCD. The flask at each step shows the solubility of the CD derivatives at room temperature before and after the complexation (photos were taken by one of the authors, Tanzeel Ur Rehman).

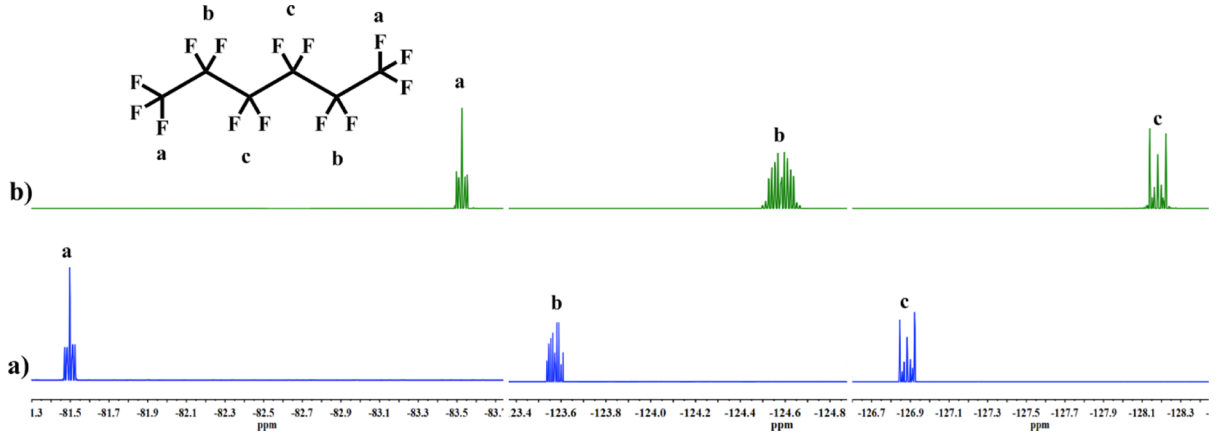

Figure 2. ^{19}F NMR spectrum of (a) NCs recorded in dimethyl sulfoxide (DMSO-d_6) and (b) PFH without using the solvent. Trifluoroacetic acid in $CDCl_3$ was inserted into the NMR tube as internal ^{19}F chemical shift standard.

RESULTS AND DISCUSSION

Preparation of NCs through Host−Guest Interactions. Initially, NCs formation was examined using BCD and PFH because BCD is the most commonly used CD derivative to form inclusion complexes with PFC derivatives. PFH was chosen as the PFC derivative because it was shown that PFH provides sustainable cavitation nuclei and allows generation of well-defined lesions at different frequencies.[13] Even though PFP (bp ≈ 29 °C, surface tension ≈ 9.5 mN/m) lowers cavitation threshold pressure ∼1−3 MPa more than PFH (bp ≈ 56 °C, surface tension ≈ 11.9 mN/m), obtaining sustainable cavitation nuclei and well-defined lesions are assessed as more important in order to have control over NMH treatments. Host−guest interaction between BCD and PFH was investigated at different BCD/PFH molar ratios of 1:1, 1:5, 1:20, and 1:50, by dissolving BCD in water at 80 °C, to ensure complete solubility, and cooled down to a temperature (45 °C) lower than boiling point of PFH before its addition. The complexation efficiency of the NCs was calculated using gas chromatography (GC). A calibration curve was constructed within a concentration range, including minimum and maximum PFH amounts that can be loaded into the BCD cavity, and the area of this known concentration of PFH was compared to the area of anisole, which was used as an internal standard at constant concentration for each measurement (Figure S1). For each NCs sample, the complexation efficiency was different and varied significantly from each other. For 1:1, 1:5, 1:20, and 1:50, the complexation efficiency turned out to be 68 ± 9, 31 ± 7, 27 ± 2, and 89 ± 21%, respectively. Increasing the ratio to 1:50 resulted in a higher complexation efficiency, but the variations in the results were high as well. It was observed that because of its lower solubility in water at room temperature (18.5 mg/mL), BCD started precipitating once the temperature was below 60 °C. This heterogeneity might cause the inconsistency of the complexation efficiency because the solution was already heterogeneous, and most of the BCD dissolved in water was already precipitated at the time of PFH addition (Figure 1a).

Thus, increasing water solubility of BCD would help us verify the above statement. To address this point and increase the complexation efficiency, the solubility of BCD was increased by a simple process of random methylation of BCD as a common and practical method in the literature. Methylation of BCD was performed using dimethyl carbonate anhydrous (DMC) and K_2CO_3 by dissolving BCD in dimethylformamide anhydrous (DMF).[41−43] The structural confirmation and degree of methylation of BCD were analyzed using nuclear magnetic resonance and mass spectroscopy, respectively. There was a clear peak shift, and −OH peaks diminished on the ^1H NMR spectrum of MCD (Figure S2) and the carbon signal of the incorporated methyl group can be clearly seen in the ^{13}C NMR spectrum (Figure S3) as well. The mass spectrum of MCD indicated high population of low degree of methylation such as 2,4,6,8-methyl groups per

DOI: 10.1021/acsomega.8b02922
ACS Omega 2019, 4, 4176−4184

molecule (Figure S4), and this was enough to significantly increase the solubility in aqueous medium. The mixture of MCD and PFH in water at room temperature resulted in a completely clear solution, followed by fine precipitate of their complex as NCs that can be taken by simple filtration and dried out as solid powder (Figure 1b). The way of using low-degree methylated BCD allowed us to establish an efficient synthesis and practical purification way for NCs preparation. Because the host molecule is completely soluble at room temperature and more available for the guest molecule, the amount of PFH used for complexation was lowered. For the molar ratios of 1:2 and 1:5 (MCD/PFH), the complexation efficiencies were revealed to be 97 ± 2 and 98 ± 3%, respectively, which accounts for approximately absolute complexation with a reasonable value of gravimetric yield comprising 40 ± 3% for 1:2 and 71 ± 7% for 1:5. This is sufficient evidence to argue for practical and economical production of a new histotripsy agent. However, to see the effect of the MCD/PFH ratio on the complexation, the amount of PFH was increased to 1:10 (MCD/PFH) and the complexation efficiency was calculated as 130 ± 4% with the gravimetric yield of 68 ± 4%, indicating the possibility of having more than one PFH molecule in the cavity of MCD when the concentration of PFH is further increased. A MCD/PFH ratio of 1:5 was chosen as the most effective ratio because it provides the uniform sample of 1:1 complexation with a higher gravimetric yield and high complexation efficiency that will allow the calculation of the PFH amount more accurately.

Characterizations of the NCs. The NCs, which refers to the inclusion complex of methylated BCD and PFH, were first characterized using NMR spectroscopy. Even though 3 and 5 protons of glucopyranose units of MCD which lie inside the cavity and 6 which lies at the minor border of the cavity did not show significant peak shift at ^{1}H NMR (Figure S5), ^{19}F NMR clearly confirmed the presence of fluorine of PFH in the NCs (Figure 2a). The spectrum of NCs showed peaks of fluorine, which confirms the development of the complex, as MCD contains no fluorine atoms. Moreover, a clear peak shift can be seen in the spectrum of NCs when compared to the spectrum of free PFH (Figure 2b). As can be seen, examining the $\Delta\delta$ ppm values for the peaks of CF_3 and CF_2, labeled as a, b, and c, listed in Table S1, all the peaks showed down field shift, and the peak a, which represents the peak of CF_3, has the highest $\Delta\delta$ ppm value (1.485), followed by peak b (1.297) and then peak c (1.074). This is consistent with the data of Gou et al. confirming the formation of the complex.[32]

Fourier transform infrared (FTIR) was performed to confirm the methylation of BCD and the formation of NCs. The FTIR spectrum of BCD, MCD, PFH, and NCs are presented in Figure S6. The spectrum of BCD showed a characteristic peak at 3200−3400 cm^{-1} because of the O−H group stretching. The characteristic peak at 2854 cm^{-1} is seen because of C−H asymmetric/symmetric stretching. Additionally, a peak at 1643 cm^{-1} represented the H−O−H deformation bands of water present in the BCD cavity. Peaks at 1152 and 1022 cm^{-1} indicated C−H overtone stretching.[44] The spectrum of MCD shows all the above characteristic peaks of BCD. According to the literature, for PFH, the characteristic peaks of CF_2 appear at 1230 and 1150 cm^{-1}, whereas the characteristic peak of CF_3 appears at 1210 cm^{-1}.[34,45−47] The same characteristic peaks were seen in the FTIR spectrum of PFH as 1235, 1143, and 1199 cm^{-1} (Figure S6). Although, the peak at 1143 cm^{-1} was overlapping with the peak of BCD and MCD, clear peaks can be seen at 1242 cm^{-1} in the spectrum of NCs, indicating the presence of PFH in the cavity, hence providing evidence for the formation of the complex.

Thermal gravimetric analysis (TGA) of NCs was performed to investigate the thermal behavior of the complex and to evaluate the low boiling point of PFH evaporation from the system. Figure 3 shows the comparison of TGA thermograms

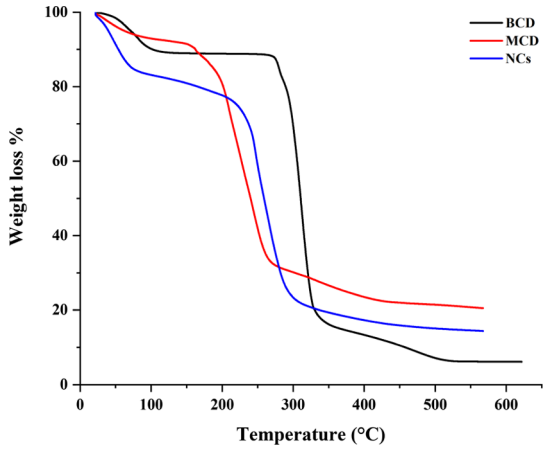

Figure 3. TGA of BCD, MCD, and NCs.

of BCD, MCD, and NCs. The first stage of BCD's thermogram was around 25−110 °C, with the midpoint of 73.0 °C indicating weight loss due to water evaporation, which was calculated as 9.55%, whereas the thermogram of MCD showed a weight loss of 7.68% for the same region at the midpoint of 62.2 °C. On the contrary, the thermogram of NCs showed higher weight loss around 19.25% at this region, and the temperature of weight loss was increased from 62.2 to 72.1 °C, indicating the presence of PFH in the structure. This increase in weight loss indicates the low boiling point (56 °C) PFH evaporation from the cavity that was also confirmed by differential scanning calorimetry (DSC) analysis presented in Figure S7. When the contribution of water evaporation of MCD on weight loss was subtracted from the weight loss of NCs, the obtained weight loss evaluated as weight loss associated with PFH evaporation. This information was used to calculate complexation efficiency as 93%, which supported the data obtained from GC. After initial weight loss because of either water or PFH evaporation, BCD, MCD, and NCs exhibited main degradation at around 315, 300, and 260 °C, respectively.

To obtain further proof of inclusion complex formation, change on the morphology and the elemental analysis of the samples were conducted via scanning electron microscopy (SEM) and energy-dispersive X-ray spectroscopy (EDX). Figure 4 shows the images at high and low magnifications of BCD, MCD, and NCs, including elemental analysis data and elemental mapping of the NCs. As can be seen in the figure, methylation of CD caused morphology change supported by the EDX data that showed increase in the atomic ratio of C as well. While BCD showed the atomic ratio of C as 43.87%, and the atomic ratio of O as 56.13%, MCD showed 63.65 and 34.19%, respectively (Figure 4a,c). An elemental analysis of the NCs made of MCD and PFH showed the atomic ratio of C as 61.25%, the atomic ratio of O as 34.14%, and the atomic ratio of F as 4.35%, indicating presence of PFH in the structure

DOI: 10.1021/acsomega.8b02922
ACS Omega 2019, 4, 4176−4184

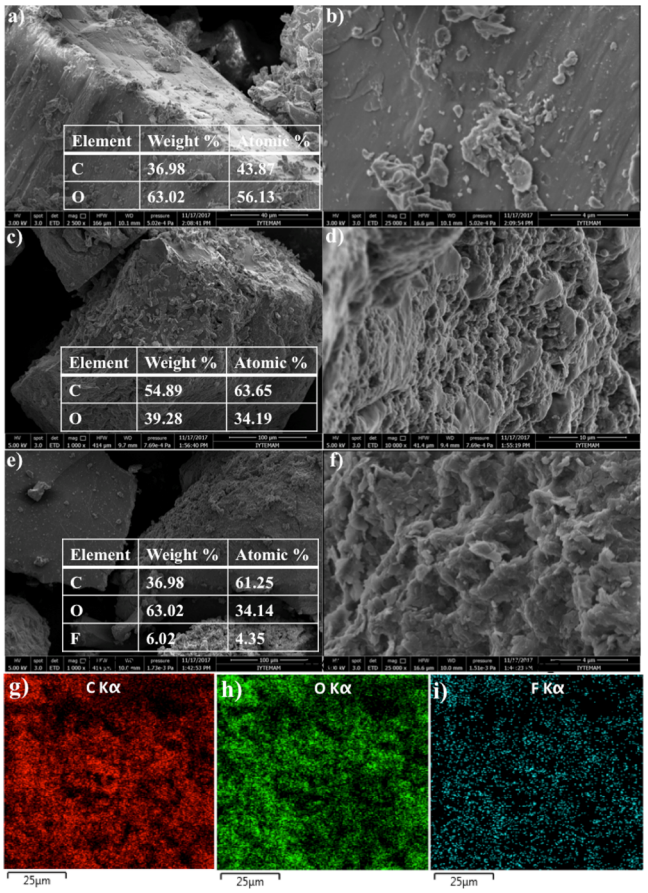

Figure 4. SEM images of dried powder samples of BCD (a) low (b) high magnification, MCD (c) low (d) high magnification, NCs formed through the inclusion complex (e) low (f) high magnification, EDX mapping of NCs (g) carbon, (h) oxygen, (i) fluorine. Elemental analyses of EDX data are presented as a table integrated into the low magnification image of each compounds.

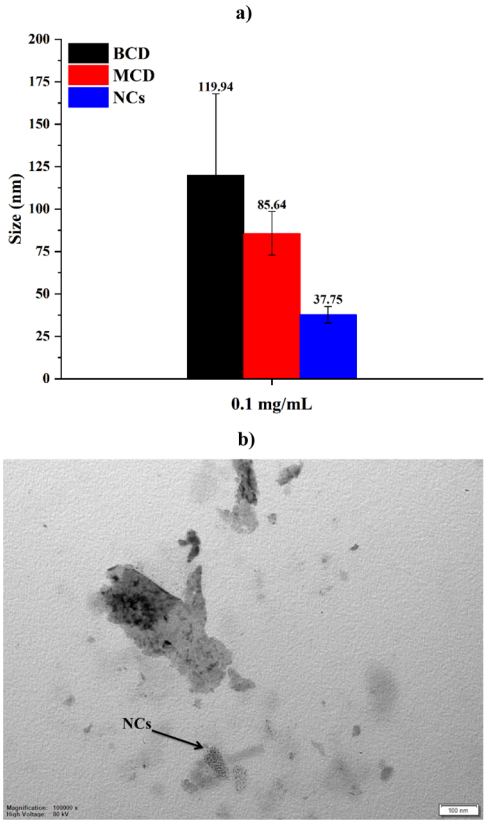

Figure 5. (a) DLS measurement comparison of size of BCD, MCD, and NCs using their 0.1 mg/mL solution in water, (b) TEM image of a 0.1 mg/mL solution of NCs showing size distribution on a scale of 100 nm.

through complex formation (Figure 4e). Moreover, a clear difference was seen in the micrograph of NCs, which showed a small platelike structure, compared to the MCD and BCD (Figure 4f). EDX is a useful technique that allows identifying the few atom thickness nanostructures to see the elemental distribution. Figure 4g–i shows that the elemental mapping of NCs showed the continuous distribution of the fluorine atom throughout the sample. NCs prepared with the MCD/PFH ratio of 1:5 and 1:10 were also analyzed via EDX (Figure S8) to compare fluorine percentage, and the results revealed that the NCs with 1:10 contained almost 25% more fluorine content than NCs with 1:5, which is correlated with the data obtained from GC.

As stated before in the hypothesis of the work, NCs are expected to have a smaller size than NDs. The size of NCs was examined using 0.1 mg/mL aqueous solution of NCs via two different methods, that is, dynamic light scattering (DLS) (Figure 5a) and transmission electron microscopy (TEM) (Figure 5b). According to the DLS results, the size of BCD and MCD were measured as 119.94 ± 47 nm, and 85.64 ± 13 nm, respectively. Low water solubility of BCD resulted in a bigger size with a large error bar, while improved solubility of MCD caused decrease in the size. The size of the NCs was 37.75 ± 7 nm, indicating better dispersion in water correlated with the published data that show inclusion complexes may have smaller size than their CD derivatives[48] (Figure 5a). In addition to DLS measurements, the size of the NCs was confirmed through an imaging technique. A well-dispersed NCs solution at a given concentration was dropped on the TEM grids and dried out before imaging. It was observed that NCs appear as very small spots on a scale of 100 nm, and it can be concluded that the size of the NCs is certainly lower than 50 nm (Figure 5b).

Biocompatibility of the NCs. Biocompatibility is one of the most important properties for any agent that is designed relying on the systemic blood circulation. An ideal agent is expected to not hemolyze the red blood cells (RBC) and to not affect the viability of the healthy cells. Even though BCD is an FDA-approved compound and PFCs are not metabolized in the body, they can be removed simply via inhalation;[18] NCs were still tested for their hemolytic activity and cell viability to provide evidence that methylation and complex formation do not change the biocompatibility of the compounds. First, the interaction between NCs and RBCs was investigated to see whether NCs cause hemolysis on RBCs. To eliminate any additional absorption apart from the free hemoglobin absorption, the plasma layer was removed from the blood sample and replaced with sodium chloride solution. The hemolytic activity of the NCs was examined via the RBCs interaction comparison of BCD, MCD, and NCs at 0.1, 0.5, and 1.0 mg/mL concentrations, and the results are presented in Figure 6. For concentrations of 0.1, 0.5, and 1.0 mg/mL, BCD showed a hemolysis of 10.9 ± 0.45, 9.5 ± 0.42, and 4.8 ± 0.37%, respectively. The decrease on hemolysis by increasing

DOI: 10.1021/acsomega.8b02922
ACS Omega 2019, 4, 4176–4184

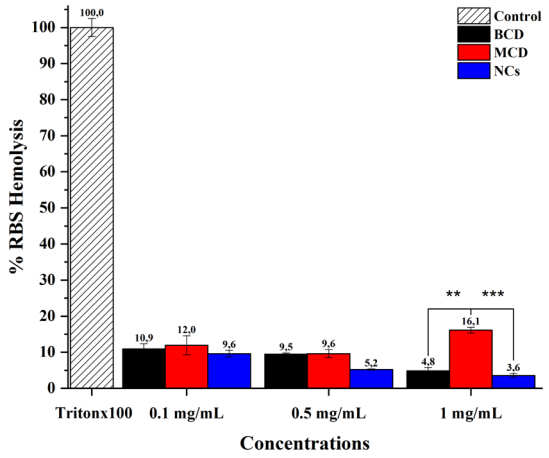

Figure 6. Percentage hemolysis caused by BCD, MCD, and NCs at different concentration. Statistical difference between percentage hemolysis was evaluated using the two-way ANOVA plus Tukey postcomparison test, where ** denotes $p \leq 0.01$ and *** denotes $p \leq 0.001$.

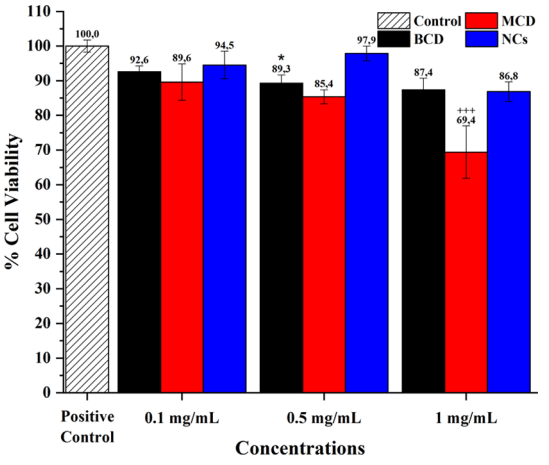

Figure 7. Cell viability of HEK-293T cells after incubation with different concentrations of BCD, MCD, and NCs. *$p < 0.02$ for BCD 0.5 mg/mL vs MCD 1 mg/mL; $^{+++}p < 0.001$ for MCD 1 mg/mL vs positive control (two-way ANOVA plus Tukey postcomparison test).

concentration of BCD is associated with aqueous solubility of BCD because high concentration of BCD results in larger aggregates in phosphate buffer solution (PBS) (data not shown), decreasing the overall particle concentration. Hence, a lower number of BCD particles interacts with the RBCs, resulting in a lower hemolysis percentage. The increase in the concentration of MCD, on the other hand, revealed the hemolysis percentage to be 11.9 ± 0.46, 9.6 ± 0.41, and 16.1 ± 0.32% for the similar concentrations, respectively, because of the increasing number of methyl groups on the outer surface of the CD, which results in slightly increased hemolytic activity of MCD. Furthermore, MCD has better water solubility than BCD, and increase in hemolysis by increasing concentration indicates the real behavior of the compound. The lowest hemolysis was caused by the NCs at each of these concentrations. At a concentration of 0.1 mg/mL, only a hemolysis of 9.6 ± 0.43% was recorded, and at 0.5 and 1.0 mg/mL, a hemolysis of 5.2 ± 0.34, and 3.1 ± 0.34%, respectively, were recorded. Decrease in hemolytic activity while increasing concentration of NCs was slightly more noticeable than decrease in hemolytic activity of BCD by the same effect. This is consistent with the data in the literature that inclusion complexes are less hemolytic than host molecules.[49] Even though it is not statistically significant, the decrease in hemolytic activity by increased concentration can be attributed to the slight increase in size (79.14 nm, see in Figure S9), which lowers NCs cell interaction.

Second, cellular cytotoxicity of NCs was investigated on healthy human embryonic kidney cells, HEK-293T, which are the cells that almost all reagent injected into body somehow passes by, as these cells will be responsible for cleaning out any trace of NCs. For this purpose, similar concentrations of 0.1, 0.5, and 1.0 mg/mL were tested for BCD, MCD and NCs. The selected concentrations were high enough to show any dose-dependent cytotoxicity of NCs. Thus, if necessary, the concentration of the NCs, which is directly proportional to the concentration of PFH, can be increased up to 1.0 mg/mL to further reduce the cavitation threshold. Figure 7 displays the results of the cell viability of each material at different concentrations. It was revealed that, upon incubation of the cells with the NCs, the cells were more viable than any other compound. For concentrations of 0.1 mg/mL, the NCs showed 94.5% cell viability, whereas BCD and MCD showed 92.6 and 89.6%, respectively. The results were similar for 0.5 mg/mL as they showed 89.3% cell viability for BCD, 85.4% for MCD, and 97.9% for the NCs. For 1.0 mg/mL, the cell viabilities of BCD and the NCs were comparable as 87.4 and 86.8% cells were viable. MCD showed a decrease in the cell viability at 1.0 mg/mL, which was calculated as 69.4% that was consistent with the hemolysis data. Overall, NCs show better cell viability than their precursors.

Histotripsy Efficiency and the Effect on the Cavitation Pressure Threshold. It was hypothesized that NCs will cause cavitation at lower cavitation pressure threshold, similar to NDs used in previous NMH experiments. This hypothesis was tested by applying single-cycle 500 kHz histotripsy pulses to the agarose gels phantom using pulse repetition frequency of 1 Hz at peak negative pressures of 16.0, 20.5, and 28.5 MPa. The corresponding peak positive pressure values were 18.8, 25.0, and 34.4 MPa, respectively. A 500 kHz transducer was used with 5 cycles per pulse. Tissue-mimicking phantoms were used to provide a well-controlled viscoelastic medium, which is very important for the study as the damage in the tissue induced by the histotripsy highly depends on the mechanical properties of the tissue.[14] Three different tissue-mimicking phantoms were prepared, including 0.7, 7 μg NCs/mL as the sample, and the empty phantom as the negative control (Figure 8). Results showed that histotripsy pulses did not create significant bubbles in the empty phantom until 28.5 MPa, which is the pressure that corresponds to the threshold cavitation pressure of normal histotripsy without an agent. Similar histotripsy applications on the phantoms that contain 0.7 and 7 μg NCs/mL, which correspond to 1×10^{-4} and 1×10^{-3} μL PFH/mL, caused bubble formation at the transducer driving voltage as low as 45 V (16.0 MPa), showing that even a small amount of PFH inside the NCs can cavitate the histotripsy at lower pressures (Figure 8). Moreover, only MCD (empty NCs) containing phantom indicated the necessity of PFH for cavitation by not showing any cavitation at the tested, 27 MPa, pressure value (Figure S10). More theoretical and experimental work needs to be done to investigate the cavitation mechanism of NCs, as well as a full comparison of the effects of NCs concentration on the histotripsy cavitation

DOI: 10.1021/acsomega.8b02922
ACS Omega 2019, 4, 4176−4184

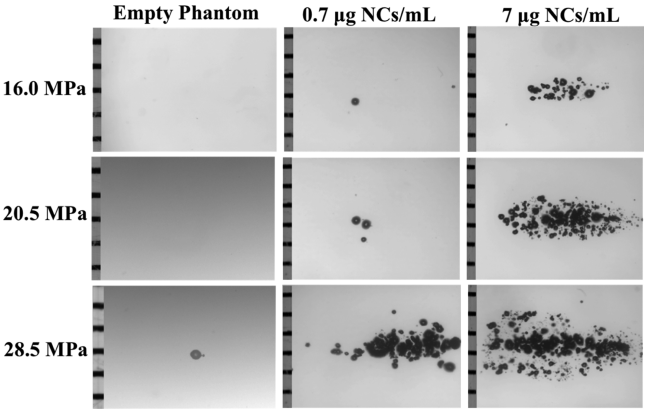

Figure 8. Bubble cloud was generated using NCs as the histotripsy agent in agarose tissue phantoms exposed to histotripsy pulses at peak negative pressures of 16.0, 20.5, and 28.5 MPa. The empty phantom was used as the negative control.

threshold including a comparison of the thresholds for NCs and our previously used NDs. These studies are currently in progress.

CONCLUSIONS

Overall, the results of this study demonstrate the feasibility of PFH-filled NCs as new generation histotripsy agents for NMH. These NCS were prepared through host−guest interaction between water-soluble derivative of CDs (MCD) and US-active PFH molecule; resulting in NMH nanoparticles that are easier to produce and more cost-/time-effective compared to the NDs used in prior NMH studies. The NCs are also smaller in size (<50 nm), which is expected to give a better chance of accumulation into the tumor tissue through the EPR effect. This is necessary for NMH to selectively ablate target tumors at lower pressures than of those used inconventional histotripsy. In addition, unlike the NDs, the PFH amount in the NCs can be directly determined in order to tune the PFH dose in planned NMH treatments, which further supports the superiority of the NCs. Additionally, the synthesis of NCs is easy, cost-effective, stable, and they are biocompatible. The NCs did not show hemolytic activity against RBCs and did not significantly affect the cell viability of the healthy human embryonic kidney cells (HEK 293T) even at the concentration as high as 1 mg/mL. Finally, NCs were able to lower the cavitation pressure threshold of histotripsy below 16.0 MPa using only 1×10^{-4} μL PFH/mL, which is a significantly smaller total volume of PFH than what was previously used in NDs-mediated histotripsy. Together, the results from this initial study demonstrate the potential of NCs for the NMH therapy, and pave the way for future studies optimizing NCs design as well as the continued development of NMH as a controllable method for targeted tumor ablation.

EXPERIMENTAL SECTION

Materials. Materials used were BCD (Sigma-Aldrich, 97%), perfluorohexane (PFH, Sigma-Aldrich, 99%), DMC (Alfa Aesar, 99%), potassium carbonate anhydrous (K_2CO_3, Sigma-Aldrich, 99.99%), anisole anhydrous (Sigma-Aldrich, 99.7%), DMF anhydrous (Sigma-Aldrich, 99.8%), DMSO (Merck, 99%), acetone (Sigma-Aldrich, 99.5%), diethyl ether anhydrous (DEE, Sigma-Aldrich, 99%), sodium chloride anhydrous (NaCl, Wisent Bioproducts, 99%), PBS (pH 7.4, Multicell, Wisent Inc.), ethanol (Sigma-Aldrich, 99.8%), Dulbecco's modified Eagle's medium (Multicell, Wisent Inc.), fetal bovine serum (FBS) advanced, heat inactivated (FBS, Capricorn Scientific GmbH), L-glutamine 200 mM solution (29.23 mg/mL in 0.85% NaCl, Multicell, Wisent Inc.), penicillin streptomycin solution (10 000 U/mL, Multicell, Wisent Inc.), trypsin−ethylenediaminetetraacetic acid (0.25% trypsin in HBSS, Multicell, Wisent Inc.), and trypan blue solution, (Sigma-Aldrich, 0.4%).

Methylation of BCD. BCD was randomly methylated using the procedure described in Gan et al.[41] Briefly, BCD (2.64 mmol) was dissolved in anhydrous DMF (60 mL) in a two-necked round-bottom flask, which was connected to a condenser on the top. After complete dissolution of BCD, K_2CO_3 (14.5 mmol) was added to the solution. Furthermore, DMC (66 mmol) was added drop-by-drop and stirred for 24 h at 45 °C under N_2 atmosphere. Subsequently, K_2CO_3 was removed by centrifuging the solution at 2000 rpm for 5 min. The solvent was removed from the solution by vacuum distillation, during which the residue turned into a syrup-like concentration. MCD was then precipitated using acetone and rinsed three times using diethyl ether. After filtration and drying process, the obtained solid was crystallized in water, filtered, and washed with acetone. The solid product was dried under vacuum and stored at room temperature before use. ^{1}H NMR (500 MHz, DMSO-d_6, δ): 5.85−5.61 (m, −O*H*2,3), 4.87−4.78 (m, 7H, *H*1), 4.45 (br, −O*H*6), 3.71−3.49 (m, *H*3,6,5), 3.43−3.24 (m, *H*4,2, −OC*H*$_3$); ^{13}C NMR (126 MHz, DMSO-d_6, δ): 102.39 (*C*1), 81.99 (*C*4), 73.90−72.04 (*C*2,3,5), 69.20 (*C*3−OCH$_3$), 67.51−67.13 (*C*6−OCH$_3$), 60.37 (*C*6, *C*2−OCH$_3$).

Preparation of NCs Using MCD and PFH. MCD (4.4×10^{-2} mmol) was dissolved in double-distilled water (1 mL) at room temperature and PFH at different molar ratios (1, 5, 10 folds) was added to the vial of MCD followed by gradual precipitation of the NCs as the product. After overnight stirring, the solutions were placed in the fridge at 4 °C for 1 h, and then centrifuged at 5000 rpm for 10 min. The supernatant was decanted and the precipitate was dried under vacuum. ^{1}H NMR (500 MHz, DMSO-d_6, δ): 5.73 (br, −O*H*2,3), 4.87−4.78 (m, 7H, *H*1), 4.47 (br, −O*H*6), 3.72−3.50 (m, *H*3,6,5), 3.44−3.26 (m, *H*4,2, −OC*H*$_3$).

Determination of Hemocompatibility. The plasma supernatant of human blood (8 mL) was discarded after centrifuging at 3500 rpm for 5 min. The RBCs were washed three times using a 150 mM saline solution. After the third wash, the RBCs solution was resuspended in 100 mM PBS (pH 7.4), followed by 10-fold dilution using PBS. Solutions of desired concentrations of the NCs (1.0, 0.5, and 0.1 mg/mL) were prepared in PBS pH 7.4 and mixed with 400 μL of RBCs solution and PBS to reach 2 mL final volume. Each solution was prepared as triplicate, as well as control solutions. The solutions were incubated at 37 °C for 1 h. After incubation, the RBCs solutions were centrifuged at 13 000 rpm for 5 min, resulting in intact and ruptured RBCs to pellet out, leaving the hemoglobin in the supernatant solution. The supernatant (200 μL) was transferred to a 96-well plate from each tube, and absorbance was measured at 541 nm as an indication of hemolysis. The observed hemolysis of untreated RBCs in PBS solution and in 0.1% v/v Triton X-100 solution was used as negative and positive controls, respectively. The observed hemolytic activity was normalized with respect to control groups.

DOI: 10.1021/acsomega.8b02922
ACS Omega 2019, 4, 4176−4184

Cell Toxicity Studies. For the cell toxicity and cell viability studies, human embryonic kidney cells (HEK-293T) were selected because of their reliable growth and propensity for transfection. Also, once the NCs are injected into blood circulation, they will eventually interact with these cells inside the body. The concentrations of 1.0, 0.5, and 0.1 mg/mL were tested on HEK-293T cells. Briefly, HEK-293T were seeded in 96-well plates at a seeding density of 20 000 cells/well and allowed to adhere overnight before replacing the culture medium with FBS-free culture medium, containing different concentrations of BCD, MCD, and NCs (1.0, 0.5, and 0.1 mg/mL), and incubating for 24 h under normal culture conditions. The medium of the cells were then replaced with 10 μL Cell Titer 96 Aqueous One Solution Cell Proliferation Assay (MTS assay reagent) containing 110 μL medium and incubated for 2 h, followed by measuring the absorbance of this solution at 490 nm using the SpectraMax i3 microplate reader. Contribution of free culture medium was eliminated by subtracting the absorbance of equal volume of culture medium at this wavelength and cell viability calculated with respect to untreated controls. The concentrations that result in statistically significant reduction in cell viability were considered cytotoxic.

Ablation of the Agarose Tissue Phantom Using NCs as a Histotripsy Agent. The phantom was made using 1% agarose w/v by slowly mixing agarose powder (Agarose type VII, Sigma-Aldrich) into saline solution. The temperature of the solution was raised above 70 °C until the solution became completely transparent. The solution was then degassed using a partial pressure vacuum of 2.7 kPa for 30 min. The agarose solution was then cooled down to 37 °C. To obtain phantoms containing NCs, they were slowly added to different gel solutions at around 40 °C while the solution was still stirring and cooling down. The agarose mixture was then poured into rectangular molds made of polycarbonate and placed at 4 °C. The solutions were allowed to solidify, and the tissue phantoms embedded with NCs (test) and without the NCs (negative control) were obtained. A 500 kHz transducer was used to apply single-cycle histotripsy pulses, and the pulse repetition frequency was set to 1.0 Hz. The results were recorded using a high-speed camera.

■ ASSOCIATED CONTENT

Supporting Information

The Supporting Information is available free of charge on the ACS Publications website at DOI: 10.1021/acsomega.8b02922.

Information of equipment and measurement conditions, hydrogen and carbon nuclear magnetic resonance spectra (^{1}H NMR and ^{13}C NMR) of NCs and MCD and ^{19}F NMR shift of NCs, mass spectroscopy analysis of MCD, FTIR spectra of BCD, MCD, NC and PFH, GC analysis of NCs and PFH calibration curves, DSC results of BCD, MCD and NCs, SEM−EDX results of NCs at different ratios, DLS results of BCD, MCD, and NCs, a table summarizing the zeta potential results, and a picture of bubble cloud generation in empty, MCD, and NCs containing phantom (PDF)

(PDF)

■ AUTHOR INFORMATION

Corresponding Authors

*E-mail: eliv@vt.edu (E.V.).

*E-mail: ydurmaz@medipol.edu.tr (Y.Y.D.).

ORCID

Yasemin Yuksel Durmaz: 0000-0003-2776-5807

Author Contributions

All the authors have given approval to the final version of the manuscript.

Notes

The authors declare no competing financial interest.

■ ACKNOWLEDGMENTS

The author (Y.Y.D.) thanks LOreal-UNESCO "For Women in Science" Program for financial support of this work.

■ REFERENCES

(1) Vlaisavljevich, E.; Aydin, O.; Yuksel Durmaz, Y.; Lin, K.-W.; Fowlkes, B.; ElSayed, M.; Xu, Z. Effects of Ultrasound Frequency on Nanodroplet-Mediated Histotripsy. *Ultrasound Med. Biol.* **2015**, *41*, 2135−2147.

(2) Parsons, J. E.; Cain, C. A.; Abrams, G. D.; Fowlkes, J. B. Pulsed Cavitational Ultrasound Therapy for Controlled Tissue Homogenization. *Ultrasound Med. Biol.* **2006**, *32*, 115−129.

(3) Roberts, W. W.; Hall, T. L.; Ives, K.; Wolf, J. S.; Fowlkes, J. B.; Cain, C. A. Pulsed Cavitational Ultrasound: A Noninvasive Technology for Controlled Tissue Ablation (Histotripsy) in the Rabbit Kidney. *J. Urol.* **2006**, *175*, 734−738.

(4) Xu, Z.; Fowlkes, J. B.; Rothman, E. D.; Levin, A. M.; Cain, C. A. Controlled Ultrasound Tissue Erosion: The Role of Dynamic Interaction between Insonation and Microbubble Activity. *J. Acoust. Soc. Am.* **2005**, *117*, 424−435.

(5) Xu, Z.; Fowlkes, J. B.; Ludomirsky, A.; Cain, C. A. Investigation of Intensity Thresholds for Ultrasound Tissue Erosion. *Ultrasound Med. Biol.* **2005**, *31*, 1673−1682.

(6) Parsons, J.; Cain, C.; Fowlkes, J. Spatial Variability in Acoustic Backscatter as an Indicator of Tissue Homogenate Production in Pulsed Cavitational Ultrasound Therapy. *IEEE Trans. Ultrason. Ferroelectr. Freq. Control* **2007**, *54*, 576−590.

(7) Maxwell, A. D.; Cain, C. A.; Hall, T. L.; Fowlkes, J. B.; Xu, Z. Probability of Cavitation for Single Ultrasound Pulses Applied to Tissues and Tissue-Mimicking Materials. *Ultrasound Med. Biol.* **2013**, *39*, 449−465.

(8) Vlaisavljevich, E.; Lin, K.-W.; Maxwell, A.; Warnez, M. T.; Mancia, L.; Singh, R.; Putnam, A. J.; Fowlkes, B.; Johnsen, E.; Cain, C.; et al. Effects of Ultrasound Frequency and Tissue Stiffness on the Histotripsy Intrinsic Threshold for Cavitation. *Ultrasound Med. Biol.* **2015**, *41*, 1651−1667.

(9) Maxwell, A. D.; Owens, G.; Gurm, H. S.; Ives, K.; Myers, D. D.; Xu, Z. Noninvasive Treatment of Deep Venous Thrombosis Using Pulsed Ultrasound Cavitation Therapy (Histotripsy) in a Porcine Model. *J. Vasc. Interv. Radiol.* **2011**, *22*, 369−377.

(10) Schade, G. R.; Keller, J.; Ives, K.; Cheng, X.; Rosol, T. J.; Keller, E.; Roberts, W. W. Histotripsy Focal Ablation of Implanted Prostate Tumor in an ACE-1 Canine Cancer Model. *J. Urol.* **2012**, *188*, 1957−1964.

(11) Vlaisavljevich, E.; Kim, Y.; Allen, S.; Owens, G.; Pelletier, S.; Cain, C.; Ives, K.; Xu, Z. Image-Guided Non-Invasive Ultrasound Liver Ablation Using Histotripsy: Feasibility Study in an In Vivo Porcine Model. *Ultrasound Med. Biol.* **2013**, *39*, 1398−1409.

(12) Hall, T. L.; Kieran, K.; Fowlkes, J. B.; Cain, C. A.; Roberts, W. W. Temporal Trends in the Histology of the Rabbit Kidney after Cavitational Tissue Ablation. *AIP Conference Proceedings*; AIP, 2007; Vol. *911*, pp 191−197.

(13) Vlaisavljevich, E.; Aydin, O.; Durmaz, Y. Y.; Lin, K.-W.; Fowlkes, B.; Xu, Z.; ElSayed, M. E. H. Effects of Droplet Composition

DOI: 10.1021/acsomega.8b02922
ACS Omega 2019, 4, 4176−4184

on Nanodroplet-Mediated Histotripsy. *Ultrasound Med. Biol.* **2016**, *42*, 931−946.
(14) Vlaisavljevich, E.; Durmaz, Y. Y.; Maxwell, A.; ElSayed, M.; Xu, Z. Nanodroplet-Mediated Histotripsy for Image-Guided Targeted Ultrasound Cell Ablation. *Theranostics* **2013**, *3*, 851−864.
(15) Yuksel Durmaz, Y.; Vlaisavljevich, E.; Xu, Z.; Elsayed, M. Development of Nanodroplets for Histotripsy-Mediated Cell Ablation. *Mol. Pharm.* **2014**, *11*, 3684−3695.
(16) Vlaisavljevich, E.; Aydin, O.; Lin, K.-W.; Durmaz, Y. Y.; Fowlkes, B.; ElSayed, M.; Xu, Z. The Role of Positive and Negative Pressure on Cavitation Nucleation in Nanodroplet-Mediated Histotripsy. *Phys. Med. Biol.* **2016**, *61*, 663−682.
(17) Aydin, O.; Vlaisavljevich, E.; Yuksel Durmaz, Y.; Xu, Z.; ElSayed, M. E. H. Noninvasive Ablation of Prostate Cancer Spheroids Using Acoustically-Activated Nanodroplets. *Mol. Pharm.* **2016**, *13*, 4054−4065.
(18) Shiraishi, K.; Endoh, R.; Furuhata, H.; Nishihara, M.; Suzuki, R.; Maruyama, K.; Oda, Y.; Jo, J.-i.; Tabata, Y.; Yamamoto, J.; et al. A Facile Preparation Method of a PFC-Containing Nano-Sized Emulsion for Theranostics of Solid Tumors. *Int. J. Pharm.* **2011**, *421*, 379−387.
(19) Wilson, K.; Homan, K.; Emelianov, S. Biomedical Photoacoustics beyond Thermal Expansion Using Triggered Nanodroplet Vaporization for Contrast-Enhanced Imaging. *Nat. Commun.* **2012**, *3*, 618.
(20) Huang, Y.; Vezeridis, A. M.; Wang, J.; Wang, Z.; Thompson, M.; Mattrey, R. F.; Gianneschi, N. C. Polymer-Stabilized Perfluorobutane Nanodroplets for Ultrasound Imaging Agents. *J. Am. Chem. Soc.* **2017**, *139*, 15−18.
(21) Sheeran, P. S.; Matsuura, N.; Borden, M. A.; Williams, R.; Matsunaga, T. O.; Burns, P. N.; Dayton, P. A. Methods of Generating Submicrometer Phase-Shift Perfluorocarbon Droplets for Applications in Medical Ultrasonography. *IEEE Trans. Ultrason. Ferroelectr. Freq. Control* **2017**, *64*, 252−263.
(22) Sheeran, P. S.; Luois, S.; Dayton, P. A.; Matsunaga, T. O. Formulation and Acoustic Studies of a New Phase-Shift Agent for Diagnostic and Therapeutic Ultrasound. *Langmuir* **2011**, *27*, 10412−10420.
(23) Yoo, K.; Walker, W. R.; Williams, R.; Tremblay-Darveau, C.; Burns, P. N.; Sheeran, P. S. Impact of Encapsulation on in Vitro and in Vivo Performance of Volatile Nanoscale Phase-Shift Perfluorocarbon Droplets. *Ultrasound Med. Biol.* **2018**, *44*, 1836−1852.
(24) Cabral, H.; Makino, J.; Matsumoto, Y.; Mi, P.; Wu, H.; Nomoto, T.; Toh, K.; Yamada, N.; Higuchi, Y.; Konishi, S.; et al. Systemic Targeting of Lymph Node Metastasis through the Blood Vascular System by Using Size-Controlled Nanocarriers. *ACS Nano* **2015**, *9*, 4957−4967.
(25) Santiesteban, D. Y.; Dumani, D. S.; Profili, D.; Emelianov, S. Y. Copper Sulfide Perfluorocarbon Nanodroplets as Clinically Relevant Photoacoustic/Ultrasound Imaging Agents. *Nano Lett.* **2017**, *17*, 5984−5989.
(26) Davis, M. E.; Brewster, M. E. Cyclodextrin-Based Pharmaceutics: Past, Present and Future. *Nat. Rev. Drug Discovery* **2004**, *3*, 1023−1035.
(27) Chaudhary, V. B.; Patel, J. K. Cyclodextrin Inclusion Complex To Enhance Solubility of Poorly Water Soluble Drugs: A Review. *Int. J. Pharma Sci. Res.* **2013**, *4* (4), 68−76.
(28) Kamitori, S.; Matsuzaka, O.; Kondo, S.; Muraoka, S.; Okuyama, K.; Noguchi, K.; Okada, M.; Harada, A. A Novel Pseudo-Polyrotaxane Structure Composed of Cyclodextrins and a Straight-Chain Polymer: Crystal Structures of Inclusion Complexes of β-Cyclodextrin with Poly(trimethylene oxide) and Poly(propylene glycol). *Macromolecules* **2000**, *33*, 1500−1502.
(29) Tiwari, G.; Tiwari, R.; Rai, A. Cyclodextrins in Delivery Systems: Applications. *J. Pharm. BioAllied Sci.* **2010**, *2*, 72.
(30) Yang, G.-F.; Wang, H.-B.; Yang, W.-C.; Gao, D.; Zhan, C.-G. Bioactive Permethrin/β-Cyclodextrin Inclusion Complex. *J. Phys. Chem. B* **2006**, *110*, 7044−7048.
(31) Song, L.-X.; Wang, H.-M.; Teng, C.-F.; Bai, L.; Xu, P.; Guo, X.-Q. Theoretical and Experimental Studies of the Inclusion Phenomena ofβ-Cyclodextrin with Organic Amines. *Chin. J. Chem.* **2008**, *26*, 1702−1708.
(32) Guo, W.; Fung, B. M.; Christian, S. D. NMR Study of Cyclodextrin Inclusion of Fluorocarbon Surfactants in Solution. *Langmuir* **1992**, *8*, 446−451.
(33) Zhang, H.; Hogen-Esch, T. E.; Boschet, F.; Margaillan, A. Complex Formation of β-Cyclodextrin- and Perfluorocarbon-Modified Water-Soluble Polymers. *Langmuir* **1998**, *14*, 4972−4977.
(34) Karoyo, A. H.; Borisov, A. S.; Wilson, L. D.; Hazendonk, P. Formation of Host-Guest Complexes of β-Cyclodextrin and Perfluorooctanoic Acid. *J. Phys. Chem. B* **2011**, *115*, 9511−9527.
(35) Karoyo, A. H.; Sidhu, P. S.; Wilson, L. D.; Hazendonk, P.; Borisov, A. Counterion Anchoring Effect on the Structure of the Solid-State Inclusion Complexes of β-Cyclodextrin and Sodium Perfluorooctanoate. *J. Phys. Chem. C* **2015**, *119*, 22225−22243.
(36) Karoyo, A. H.; Sidhu, P.; Wilson, L. D.; Hazendonk, P. Characterization and Dynamic Properties for the Solid Inclusion Complexes of β-Cyclodextrin and Perfluorobutyric Acid. *J. Phys. Chem. C* **2014**, *118*, 15460−15473.
(37) Yao, Y.; Liu, X.; Liu, T.; Zhou, J.; Zhu, J.; Sun, G.; He, D. Preparation of inclusion complex of perfluorocarbon compound with β-cyclodextrin for ultrasound contrast agent. *RSC Adv.* **2015**, *5*, 6305−6310.
(38) Loftsson, T.; Brewster, M. E. Pharmaceutical Applications of Cyclodextrins. 1. Drug Solubilization and Stabilization. *J. Pharm. Sci.* **1996**, *85*, 1017−1025.
(39) Gidwani, B.; Vyas, A. A Comprehensive Review on Cyclodextrin-Based Carriers for Delivery of Chemotherapeutic Cytotoxic Anticancer Drugs. *Biomed Res. Int.* **2015**, *2015*, 1−15.
(40) Loftsson, T.; Jarho, P.; Másson, M.; Järvinen, T. Cyclodextrins in Drug Delivery. *Expert Opin. Drug Delivery* **2005**, *2*, 335−351.
(41) Gan, Y.; Zhang, Y.; Xiao, C.; Zhou, C.; Zhao, Y. A novel preparation of methyl-β-cyclodextrin from dimethyl carbonate and β-cyclodextrin. *Carbohydr. Res.* **2011**, *346*, 389−392.
(42) Damiani, E.; Tursilli, R.; Casolari, A.; Astolfi, P.; Greci, L.; Scalia, S. Effect of complexation with randomly methylated β-cyclodextrin on the aqueous solubility, photostability and antioxidant activity of an indolinonic nitroxide radical. *Free Radical Res.* **2005**, *39*, 41−49.
(43) Agatonovic-Kustrin, S.; Glass, B. D.; Brown, M. E.; Lebete, M. L. For and Against the Use of Methylated Cyclodextrins in the Development of Midazolam Solution for Nasal Application. *Austin J. Pharmacol. Ther.* **2014**, *2* (2), 1016.
(44) Rachmawati, H.; Edityaningrum, C. A.; Mauludin, R. Molecular Inclusion Complex of Curcumin-β-Cyclodextrin Nanoparticle to Enhance Curcumin Skin Permeability from Hydrophilic Matrix Gel. *AAPS PharmSciTech* **2013**, *14*, 1303−1312.
(45) Tatsuno, H.; Ando, S. Structure and Dynamics of Perfluoroalkane/β-Cyclodextrin Inclusion Compounds As Studied by Solid-State19F MAS and1H →19F CP/MAS NMR Spectroscopy. *J. Phys. Chem. B* **2006**, *110*, 25751−25760.
(46) Pawsey, S.; Reven, L. 19F Fast Magic-Angle Spinning NMR Studies of Perfluoroalkanoic Acid Self-Assembled Monolayers. *Langmuir* **2006**, *22*, 1055−1062.
(47) Moynihan, R. E. The Molecular Structure of Perfluorocarbon Polymers. Infrared Studies on Polytetrafluoroethylene1. *J. Am. Chem. Soc.* **1959**, *81*, 1045−1050.
(48) Lo, Y.; Hsu, C.; Tsai, T.; Cham, T. Comparison of the Solubility and Dissolution Rate of Gliclazide-Beta-Cyclodextrin Inclusion Complexes Prepared by Liquid/Liquid Extraction and Neutralization. *J. Food Drug Anal.* **2006**, *14* (3), 230−235.
(49) Koizumi, K.; Okada, Y.; Kubota, Y.; Utamura, T. Inclusion Complexes of Poorly Water-Soluble Drugs with Glucosyl-Cyclodextrins. *Chem. Pharm. Bull.* **1987**, *35*, 3413−3418.

DOI: 10.1021/acsomega.8b02922
ACS Omega 2019, 4, 4176−4184